Liquid Crystals
Publication details, including instructions for authors and subscription information:
http://www.informaworld.com/smpp/title~content=t713926090

Synthesis, mesomorphic behaviour and optoelectronic properties of phosphorus-based thermotropic liquid crystalline dendrimers

A. Iwan[ab]; H. Janeczek[c]; M. Domanski[c]; P. Rannou[b]
[a] Electrotechnical Institute, Division of Electrotechnology and Materials Science, Wroclaw, Poland [b] Laboratoire d'Electronique Moléculaire, Organique et Hybride, UMR5819-SPrAM (CEA-CNRS-Univ. J. FOURIER-Grenoble I), Institut Nanosciences et Cryogénie (INAC), Grenoble Cédex 9, France [c] Centre of Polymer and Carbon Materials, Polish Academy of Sciences, Zabrze, Poland

Online publication date: 16 August 2010

To cite this Article Iwan, A. , Janeczek, H. , Domanski, M. and Rannou, P.(2010) 'Synthesis, mesomorphic behaviour and optoelectronic properties of phosphorus-based thermotropic liquid crystalline dendrimers', Liquid Crystals, 37: 8, 1033 — 1045
To link to this Article: DOI: 10.1080/02678291003782838
URL: http://dx.doi.org/10.1080/02678291003782838

Liquid Crystals,
Vol. 37, No. 8, August 2010, 1033–1045

Taylor & Francis
Taylor & Francis Group

Synthesis, mesomorphic behaviour and optoelectronic properties of phosphorus-based thermotropic liquid crystalline dendrimers

A. Iwan[a,b]*, H. Janeczek[c], M. Domanski[c] and P. Rannou[b]

[a]*Electrotechnical Institute, Division of Electrotechnology and Materials Science, M. Sklodowskiej–Curie 55/61 Street, 50–369 Wroclaw, Poland;* [b]*Laboratoire d'Electronique Moléculaire, Organique et Hybride, UMR5819–SPrAM (CEA–CNRS–Univ. J. FOURIER–Grenoble I), Institut Nanosciences et Cryogénie (INAC), CEA–Grenoble, 17 rue des Martyrs, 38054 Grenoble Cédex 9, France;* [c]*Centre of Polymer and Carbon Materials, Polish Academy of Sciences, M. Sklodowskiej–Curie 34 Street, 41–819 Zabrze, Poland*

(*Received 19 November 2009; final version received 16 March 2010*)

A new series of thermotropic phosphorus-based liquid crystalline (LC) dendrimers based on a thiophosphoryl-phenoxymethyl(methylhydrazono) core (thiophosphoryl-PMMH) up to the fifth generation has been synthesised by solution condensation of aldehyde groups, surface-functionalised thiophosphoryl-PMMH dendritic substrates of generation numbers $G_{0.5}$ to $G_{5.5}$, with the appropriate molar equivalents of the pro-mesogenic *n*-hexadecylaniline mono-functional building block. Their chemical composition has been confirmed by $^{1}H/^{13}C/^{31}P$ nuclear magnetic resonance spectroscopy, Fourier transform infrared spectroscopy, elemental analysis. Optical properties have been studied by ultraviolet-visible absorption, photoluminescence spectroscopy and polarised optical microscopy, and thermal characteristics by differential scanning calorimetry. Electrical studies have been made using the current-voltage characteristics of organic light-emitting diodes consisting of multi-layered indium tin oxide/dendrimer/aluminium tris(8-hydroxyquinoline)Al architecture. It has been demonstrated that the molecular engineering approach adopted can successfully lead to phosphorus-containing dendritic organic semiconductors (OSCs) which show tunable mesomorphic behaviour (extension of the observed smectic mesophase) and (opto) electronic properties, owing to their peripheral decoration with a tunable number of azomethine-based optically active chromophoric units. This rare combination of 'tunable by design' properties makes this series of thermostable thiophosphoryl-PMMH-based LC dendrimers a particularly appealing class of OSCs for use in optically and/or electronically active layers of (opto)electronic devices such as light-emitting diodes, field-effect transistors, solar cells and lasers.

Keywords: phosphorus dendrimers; liquid crystalline dendrimers; azomethines; hole transporting materials

1. Introduction

Dendrimers are a fascinating recently developed subclass of hyperbranched materials [1–5]. They contain 'tunable by design and on demand' architecture which can be easily connstructed, either through 'divergent' or 'convergent' strategies, to produce advanced functional materials for a broad range of applications [1–9]. Their appealing features include their solubility in common solvents, their ease of purification and their intrinsically monodisperse character, even in the case of dendrimers of high generation numbers. Although their molecular weight is of the same order as conventional polymers, their precisely defined multi-level (core, shell and surface) chemical structures explain their successful development as versatile synthetic platforms both in fundamental research (e.g. in materials science) and also in applicational-oriented research [6–9].

Phosphorus-based dendrimers were pioneered and developed by the group led by Caminade and Majoral [10–29] and shared their useful features with other well-known types of dendrimers, including poly(benzylethers), poly(propylene imines), poly(ethylene imines) and poly(amido-amines) [1–5]. These dendrimers enable the development of functional materials with properties such as with high dipole moment [11], biocompatibility [18] and good thermal stability [17], which allow their use in new functional materials.

A recent example of the versatility of dendrimer-based synthetic platforms in materials science has been the development of functional liquid crystalline (LC) dendrimers [30–37]. This area of development has progressed rapidly over the last decade. A number of LC dendrimers based on cyclic phosphazene cores, such as cyclotriphosphazene and cyclotetraphosphazene [38–47], decorated at their periphery with (pro-)mesogenic biphenyl, azo, ester or Schiff's base units [48], have been reported. This follows earlier work on closely related liquid crystalline organophosphazene polymeric and cyclic oligomer derivatives [49–54]. While intensive efforts were being pursued by the Caminade–Majoral group and others towards the development of an

*Corresponding author. Email: a.iwan@iel.wroc.pl

ISSN 0267-8292 print/ISSN 1366-5855 online

DOI: 10.1080/02678291003782838
http://www.informaworld.com

impressive range of functional dendrimers using phosphorus-based cores (e.g. thiophosphoryl and cyclotriphosphazene) [10–29], the present authors were surprised that less attention was being paid to thiophosphoryl-based liquid crystalline dendrimers. This has led them to design, synthesise and characterise a novel series of thermotropic thiophosphoryl-phenoxymethyl (methylhydrazono) (thiophosphoryl-PMMH) LC dendrimers up to the fifth generation.

The aims of the present study were as follows:

(1) To explore the synthesis and the mesomorphic behaviour of this novel series of phosphorus-based dendrimers, decorated at their periphery by 3 to 96 pro-mesogenic azomethine-based chromophoric units;
(2) to describe the optoelectronic (UV–Vis absorption and photoluminescence (PL)) features of this group of phosphorus-containing dendritic organic semiconductors [55]; and
(3) to investigate the potential of these functional dendrimers [56–57] in the emerging field of organic (opto)electronics [58], by examining their value as hole transporting materials in the multilayered indium tin oxide (ITO)/dendrimer/aluminium tris(8-hydroxyquinoline) (Alq_3)/Al architecture of an organic light-emitting diode.

2. Experimental

2.1 Materials and characterisation techniques

All chemicals and reagents were obtained from Aldrich and were used as received.

The dendrimers were each purified by thin-layer chromatography (TLC) using Merck silica gel F254 TLC plates and a 50/50 vol/vol dichloromethane/ethyl acetate eluent. The chemical structure of the dendrimers was confirmed by elemental analysis and using ^{1}H, ^{13}C, ^{31}P nuclear magnetic resonance (NMR) and Fourier transform infrared (FTIR) spectroscopy. NMR spectra were recorded on a Bruker AC 200 MHz or a Varian Unity 400 MHz spectrometer. Dichloromethane–d_2 (CD_2Cl_2) containing TMS (tetramethylsilane) was used as solvent in determining the ^{1}H and ^{13}C NMR spectra of the dendrimers, while ^{31}P NMR spectra recorded in CD_2Cl_2 were referenced to an external 85% H_3PO_4 standard. FTIR spectra of neat dendrimers (*ca.* 1–2 mg) were recorded on a Perkin–Elmer Paragon 500 spectrometer (resolution 4 cm^{-1}) equipped with a SPECAC Golden-Gate attenuated total reflectance attachment by averaging 64 scans at room temperature (20°C). Elemental analysis (C, H, N) was carried out on a Perkin–Elmer 240C analyser.

The optoelectronic properties of the thiophosphoryl-PMMH dendrimers were investigated using steady-state UV–Vis absorption and PL spectroscopy. UV–Vis absorption spectra in tetrahydrofuran (THF) solution were recorded *in situ* during analytical size exclusion chromatography analyses (not discussed here) using the diode array detector (DAD) of a Hewlett-Packard 1100 Chemstation equipped with a 300x7.5 mm Polymer Labs PL gel Mixed–D 5 μm 10^4 Å column, and a DAD and refractive index detector. The column temperature and flow rate were maintained at 40°C and 1 mL min^{-1}, respectively. The calibration curve was constructed using 10 polystyrene narrow standards (S–M2–10* kit from Polymer Labs). Two runs of 20 μL injections of a *ca.* 0.5 mg mL^{-1} HPLC-grade THF solution of each dendrimer were assessed using a UV–Vis detector at 325 nm. Solution PL spectra were recorded on diluted THF solutions at room temperature using a Hitachi F–4500 spectrometer, showing an absorption level of. *ca.* 0.1 absorbance unit at the wavelength chosen for excitation ($\lambda_{exc} = 325$ nm).

The thermotropic LC behaviour of thiophosphoryl-PMMH-based dendrimers up to the fifth generation was investigated by means of DSC and POM. DSC thermograms were measured under a nitrogen atmosphere on a TA–DSC 2010 apparatus using sealed aluminium pans at heating/cooling rates of 0.5°C min^{-1} in the temperature range of the –20°C clearing point. The texture of the mesophases was observed by means of a POM set-up comprising: (i) a Leica DMLM microscope operating in both transmission and reflection mode and equipped with lenses giving magnification of 2.5×, 5×, 10×, 20× and 50×, (ii) a Linkam LTS350 (–196°C to +350°C) hotplate and Linkam CI94 temperature controller, and (iii) a JVC Numeric 3-CCD KYF75 camera, resolution 1360 × 1024.

Electrical measurements (current–voltage (*IV*) characteristics) of organic light-emitting diodes (OLEDs) were performed on a device having multilayered ITO/Alq_3/Al and ITO/dendrimer/Alq_3/Al architectures. Thiophosphoryl-PMMH-based dendrimer solutions (1% w/v in dichloromethane) were spin-cast on to an ITO-covered glass substrate at room temperature to produce a *ca.* 150 nm thick hole-transporting layer (HTL). Residual traces of solvent were removed by heating the thin film at 50°C for 5 h under a vacuum of *ca.* 5 Torr. An approximately 40 nm thick green-emitting Alq_3 thin layer was vacuum deposited on the HTL at a base pressure of *ca.* 10^{-6} Torr. To complete the OLED device, a *ca.* 600 nm thick low work-function aluminium electrode was vacuum deposited (base pressure *ca.* 10^{-6} Torr) through a mask on top of the emitting layer to produce an OLED area of 9 mm^2. IV characteristics were measured using a Keithley 6715 electrometer.

2.2 Thermotropic thiophosphoryl-PMMH LC dendrimers of generations 0–5 (TD0-5)

2.2.1 TD0

A mixture of thiophosphoryl-PMMH-3 dendrimer (0.1 mmol), *n*-hexadecylaniline (*n*-HAD; 0.34 mmol) and *p*-toluenesulfonic acid (PTSA; 0.1 mmol) was refluxed in chloroform (15 ml) with magnetic stirring under an atmosphere of argon for 60 h. After the mixture had been cooled to room temperature and the reaction medium evaporated to dryness, the product (yield 64%) was purified by column chromatography on silica gel (60 μm) using ethyl acetate/hexane 1/9 as eluent.

Properties: yellow solid, mp 41°C.

^{1}H NMR (200 MHz, CD_2Cl_2, ppm) δ = 8.01, 8.05 (a), 7.19, 7.23 (b), 8.55 (c), 7.44, 7.48 (d), 7.26, 7.30 (e), 2.65–2.72 (f), 1.64 (g), 1.32 (h), 0.91–0.98 (i): codes as in Figure 3.

^{13}C NMR (50 MHz, CD_2Cl_2, ppm) δ = 14.58 (i), 23.12 (n), 29.78, 29.94 (h), 32.05, 32.36 (g, o), 35.42, 35.86 (f), 115.27 (b), 121.88, 121.97 (d), 122.22, 122.31 (l), 129.55 (e), 130.61, 131.94 (a), 134.97 (k), 141.79 (j), 149.65 (m), 158.11 (c): codes as in Figure 3.

^{31}P NMR (ppm): δ = 52. ν_{max} (cm^{-1}): 2954, 2916 $\nu_{asym.}$ CH_2, 2848 $\nu_{sym.}$ CH_2, 1628 ν CH=N, 1597 ν Ph, 740 ν P=S.

Analysis: Calc. for $C_{87}H_{126}N_3O_3PS$ (1324.99): C, 78.86; H, 9.59; N, 3.17. Found: C, 78.68; H, 9.52; N, 3.10.

2.2.2 TD1

A mixture of thiophosphoryl-PMMH-6 dendrimer (0.1 mmol), *n*-HDA (0.9 mmol) and PTSA (0.1 mmol) was refluxed in chloroform (15 ml) with magnetic stirring under an atmosphere of argon for 60 h. After the mixture had been cooled to room temperature and the reaction medium evaporated to dryness, the product (yield 64%) was purified by column chromatography on silica gel (60 μm) using ethyl acetate/hexane 1/9 as eluent.

Properties: yellow solid, mp 50°C.

^{1}H NMR (200 MHz, CD_2Cl_2, ppm) δ = 6.61, 6.66 (a), 7.73 (b), 8.48 (c), 2.66 (d), 6.97–7.01 (e), 7.90 (f), 7.35 (g), 7.18–7.22 (h), 2.48–2.56 (i), 1.62 (j), 1.32 (k), 0.93 (m): codes as in Figure 2.

^{13}C NMR (50 MHz, CD_2Cl_2, ppm) δ = 12.66, 12.76 (m), 21.47 (l), 28.13, 28.31, 28.45 (k), 30.39, 30.66 (j), 33.75, 34.19 (i), 37.67 (d), 113.59, 114.16 (e), 119.46 (b), 120.30, 120.41, 120.51 (g), 127.76, 127.84 (s), 128.71, 128.93 (h), 131.53 (a), 132.65 (f), 136.08 (o), 142.91 (n), 143.16 (p), 147.94, 148.07 (r), 151.50, 152.14 (t), 156.41, 156.63 (c): codes as in Figure 2.

^{31}P NMR (ppm): δ = 52 and 62. ν_{max} (cm^{-1}): 2955, 2916 $\nu_{asym.}$ CH_2, 2848 $\nu_{sym.}$ CH_2, 1624 ν CH=N, 1598 ν Ph, 740 ν P=S.

Analysis: Calc. for $C_{198}H_{276}N_{12}O_9P_4S_4$ (3220.54): C, 73.84; H, 8.64; N, 5.22. Found: C, 73.58; H, 8.52; N, 4.99.

2.2.3 TD2

A mixture of thiophosphoryl-PMMH-12 dendrimer (0.1 mmol), *n*-HDA (1.5 mmol) and PTSA (0.1 mmol) was refluxed in chloroform (25 ml) with magnetic stirring for 110 h under argon. After the mixture had been cooled to room temperature and the reaction medium evaporated to dryness, the product (yield 65%) was purified by column chromatography on silica gel (60 μm) using ethyl acetate/hexane 1/9 as eluent.

Properties: yellow solid, mp 51°C.

^{1}H NMR (200 MHz, CD_2Cl_2, ppm) δ = 6.62, 6.66 (a), 7.73, 7.77, 7.81 (b), 8.48 (c), 2.64 (d), 6.98–7.01 (e), 7.90–8.03 (f), 7.34–7.45 (g), 7.18–7.29 (h), 2.49–2.64 (i), 1.60 (j) 1.32 (k), 0.96 (m): codes similar to those in Figure 2 for TD1.

^{13}C NMR (50 MHz, CD_2Cl_2, ppm) δ = 13.97 (m), 22.77 (l), 29.76, 29.63, 29.39 (k), 31.70 (j), 32.00 (i), 35.07, 35.51 (d), 114.91 (e), 120.80 (b), 121.84 (g), 130.05, 130.26, 132.84 (a, f, s, h, o), 141.26, 141.44 (n), 144.48 (p), 149.41 (r), 153.11 (t), 157.98 (c).

^{31}P NMR (ppm): δ = 52 and 62. ν_{max} (cm^{-1}): 2955, 2919 $\nu_{asym.}$ CH_2, 2850 $\nu_{sym.}$ CH_2, 1628 ν CH=N, 1598 ν Ph.

2.2.4 TD3

A mixture of thiophosphoryl-PMMH-24 dendrimer (0.1 mmol), *n*-HDA (2.8 mmol) and PTSA (0.1 mmol) was refluxed in chloroform (25 ml) with magnetic stirring for 130 h under argon. After the mixture had been cooled to room temperature and the reaction medium evaporated to dryness, the product (yield 69%) was purified by column chromatography on silica gel (60 μm) using ethyl acetate/hexane 1/9 as eluent.

Properties: yellow solid, mp 51°C.

^{1}H NMR (200 MHz, CD_2Cl_2, ppm) δ = 6.62, 6.66 (a), 7.74, 7.92, 7.95 (b), 8.49 (c), 2.66 (d), 6.97–7.02 (e), 7.92–7.95 (f), 7.36–7.39 (g), 7.16–7.23 (h), 2.49–2.56 (i), 1.60 (j) 1.32 (k), 0.94 (m): codes similar to those used for TD1in Figure 2.

^{13}C NMR (50 MHz, CD_2Cl_2, ppm) δ = 14.31 (m), 23.12 (l), 29.72 (k), 30.11 (j), 32.05, 32.34 (i), 35.41, 35.48 (d), 115.23 (e), 121.11 (b), 122.08, 122.17 (g), 130.36, 133.18, 134.33 (a, f, s, h, o), 141.62 (n), 144.82 (p), 149.56 (r), 153.18 (t), 158.30 (c).

^{31}P NMR (ppm): δ = 52, 59 and 62. ν_{max} (cm^{-1}): 2955, 2916 $\nu_{asym.}$ CH_2, 2849 $\nu_{sym.}$ CH_2, 1627 ν CH=N, 1600 ν Ph.

2.2.5 *TD4*

A mixture of thiophosphoryl-PMMH-48 dendrimer (0.1 mmol), *n*-HDA (10.0 mmol) and PTSA (0.1 mmol) was refluxed in chloroform (30 ml) with magnetic stirring for 150 h under argon. After the mixture had been cooled to room temperature and the reaction medium evaporated to dryness, the product (yield 68%) was purified by column chromatography on silica gel (60 μm) using ethyl acetate/hexane 1/9 as eluent.

Properties: yellow solid, mp 52°C.

^{1}H NMR (200 MHz, CD_2Cl_2, ppm) δ = 6.67, 6.71 (a), 7.73 (b), 8.48 (c), 7.00–7.04 (e), 7.86–7.91 (f), 7.30–7.32 (g), 7.16–7.21 (h), 2.49–2.57 (d, i), 1.59 (j) 1.29 (k), 0.92 (m): codes as those used for TD1 in Figure 2.

^{13}C NMR (50 MHz, CD_2Cl_2, ppm) δ = 13.47 (m), 22.03 (l), 28.65 (k), 31.18, 31.27 (i, j), 34.42 (d), 114.61 (e), 120.12, 120.43 (b), 121.23 (g), 128.48, 129.40, 132.60 (a, f, s, h, o), 143.02, 143.18 (n, p), 149.80 (r), 153.18 (t), 158.00 (c).

^{31}P NMR (ppm): δ = 52, 59 and 62. ν_{max} (cm^{-1}): 2955, 2914 $\nu_{asym.}$ CH_2, 2847 $\nu_{sym.}$ CH_2, 1624 ν CH=N, 1602 ν Ph.

2.2.6 *TD5*

A mixture of thiophosphoryl-PMMH-96 dendrimer (0.1 mmol), *n*-hexadecylaniline (21.0 mmol) and *p*-toluenesulfonic acid (0.1 mmol) was refluxed in chloroform (35 ml) with magnetic stirring for 168 h under argon. After the mixture had been cooled to room temperature and the reaction medium evaporated to dryness, the product (67% yield) was purified by column chromatography on silica gel (60 μm) using ethyl acetate/hexane 1/9 as eluent.

Properties: yellow solid, mp 53°C.

^{1}H NMR (200 MHz, CD_2Cl_2, ppm) δ = 6.66, 6.68 (a), 7.76 (b), 8.47 (c), 6.97–7.02 (e), 7.93 (f), 7.26–7.35 (g), 7.18–7.22 (h), 2.49–2.64 (d, i), 1.59 (j) 1.32 (k), 0.94 (m): codes similar to those in Figure 2 for TD1.

^{13}C NMR (50 MHz, CD_2Cl_2, ppm) δ = 12.99 (m), 21.79 (l), 28.64, 28.77 (k), 31.02 (i, j), 34.07 (d), 113.90 (e), 120.74 (b), 121.18 (g), 128.08, 129.02, 130.47, 131.64, 131.84 (a, f, s, h, o), 143.10, 143.47 (n, p), 149.80 (r), 152.84, 153.41 (t), 161.00 (c).

^{31}P NMR (ppm): δ = 52, 59 and 62. ν_{max} (cm^{-1}): 2955, 2914 $\nu_{asym.}$ CH_2, 2847 $\nu_{sym.}$ CH_2, 1626 ν HC=N, 1602 ν Ph.

3. Results

Thermotropic thiophosphoryl-PMMH-based liquid crystalline (LC) dendrimers are abbreviated in the manner **TD*n***, where n = 0–5, corresponding to the generation number G_n.

The dendrimers were synthesised by solution condensation of commercially available thiophosphoryl-phenoxymethyl(methylhydrazono) dendritic cores of generations $G_{0.5}$ to $G_{5.5}$, with 3, 6, 12, 24, 48 and 96 aldehyde (CHO) surface groups, over a pro-mesogenic *n*-HDA monofunctional substrate. A slight to moderate excess of *n*-HDA with respect to the number of aldehyde groups located at the periphery of the dendritic substrates were used (*ca.* 1.125–2.188 molar equivalents of NH_2 groups to 1 molar equivalent of CHO groups). Combined with increasing reaction time, determined by TLC monitoring to indicate completion of the reaction, this ensured complete conversion of the 3–96 surface CHO groups into a similar number of azomethine (–CH=N–) groupings [48] which decorate the periphery of the $G_{0–5}$ thermotropic thiophosphoryl-PMMH-based dendrimers **TD0–5**. The synthetic access to **TD0** and **TD1** is shown in Figure 1, and the calculated molecular weight, the weight content in azomethine-based pro-mesogenic surface groups [–CH=N–C_6H_4–$C_{16}H_{33}$], the synthetic reaction time, the generation number (G_n), the number of peripheral groups per volume unit (Z) and number of junctions (J) of thermotropic thiophosphoryl-PMMH-based LC dendrimers **TD0–5** are summarised in Table 1.

Full conversion of the 3–96 CHO surface groups into azomethine groupings [48] of the purified LC dendrimers **TD0–5** was unambiguously confirmed by means of ^{1}H, ^{13}C, ^{31}P NMR and FTIR spectroscopy and tracking the disappearance of the characteristic signals corresponding to CHO and NH_2 functions in the substrate and their replacement by signals corresponding to the –CH=N– functions of the LC dendrimers **TD0–5.** The chemical structure of **TD0–1** was additionally confirmed by elemental analysis of C, H and N. Except for the particular case of the LC dendrimer of generation G_0, the ^{1}H, ^{13}C NMR and FTIR spectra of the **TD0–5** dendrimers did not show significant variations in chemical features between the generations. The representative example of the ^{1}H NMR spectrum of the first generation dendrimer **TD1** is given in Figure 2.

The imine proton signal in the ^{1}H NMR spectra of **TD0-5** dendrimers was observed in the 8.47–8.55 ppm range. More precisely, while ^{1}H NMR spectra of dendrimers **TD1–5** showed a signal at 8.47–8.49 ppm for the imine-type proton, a slightly downward shift to 8.55 ppm was observed in the ^{1}H spectrum of the dendrimer **TD0**. Additionally, as seen in the ^{13}C NMR spectrum of **TD0** illustrated in Figure 3, ^{13}C NMR analyses of all the dendrimers revealed the presence of a signal in the 156–161 ppm range, which may be attributable to the carbon atom in the peripheral azomethine units.

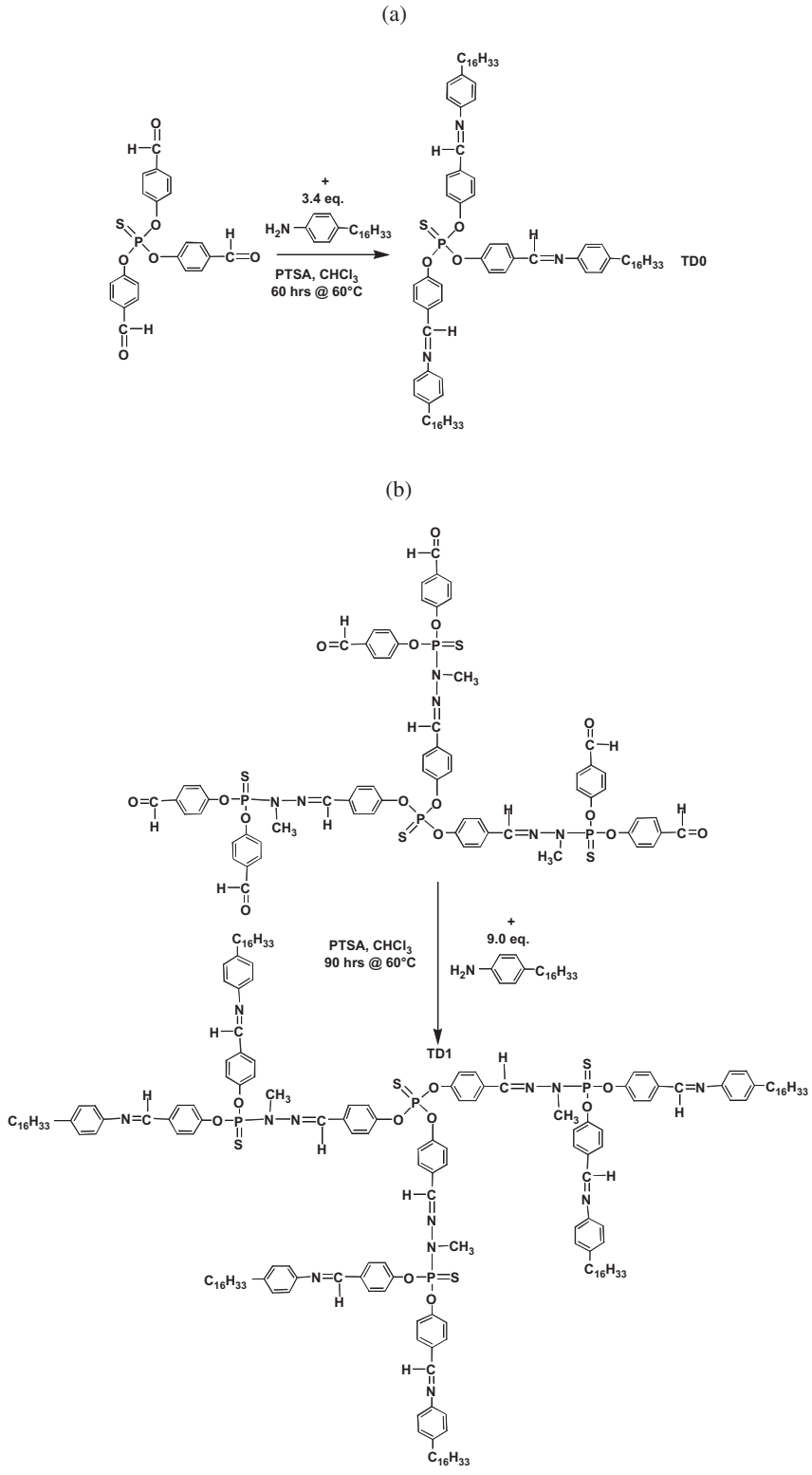

Figure 1. Synthetic access to thiophosphoryl-PMMH-based LC dendrimers of the G_0 and G_1 generations: (a) **TD0,** (b) **TD1**.

The ^{31}P NMR spectra of the dendrimers **TD0–5** showed signals related to their P=S bond. The signals were influenced by increasing generation number and the associated restricted molecular mobility (on the time scale of NMR) which increased from *ca.* 1300 g mol^{-1} to *ca.* 60 000 g mol^{-1}. Accordingly, the ^{31}P NMR spectrum of dendrimer **TD0** showed one doublet at *ca.* $\delta = 52$ ppm, typical of its $[_3(O)]$–P=S bond,

Table 1. Codes, calculated molecular weight, weight content in azomethine-based pro-mesogenic surface groups [–CH=N–C_6H_4–$C_{16}H_{33}$] and synthetic reaction time for thiophosphoryl-PMMH-based LC dendrimers up to the fifth generation, along with their calculated generation number (G_n), number of peripheral groups per unit volume ($Z = N_c \times N_b^G$), and number of junctions ($J = N_c \times [(N_b^G–1)/(N_b–1)]$).

Code	Calculated molecular weight [g mol^{-1}]	Weight content in azomethine-based pro-mesogenic surface groups [wt%]	Synthetic reaction time [h]	G_n	Z	J
TD0	1324.99	71.3	60	G_0	3	0
TD1	3220.54	58.7	90	G_1	6	3
TD2	7011.62	53.9	110	G_2	12	9
TD3	14,593.73	51.8	130	G_3	24	21
TD4	29,758.21	50.8	150	G_4	48	45
TD5	60,086.99	50.3	168	G_5	96	93

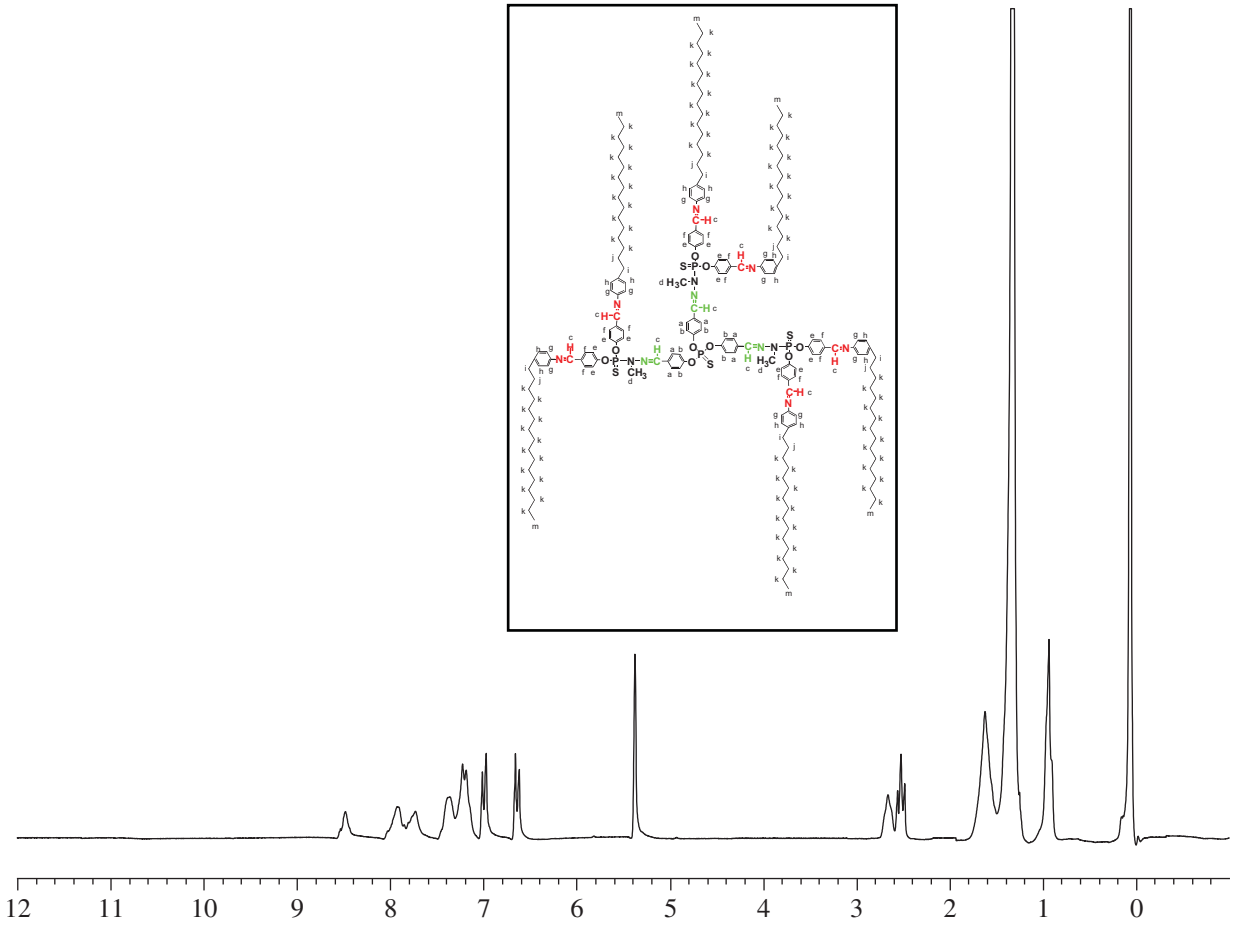

Figure 2. ^{1}H NMR spectrum of thiophosphoryl-PMMH-based LC dendrimer **TD1**. Inset: Chemical structure of **TD1** together with codes related to observed ^{1}H NMR peaks (colour version online).

while two characteristic doublets located at *ca.* $\delta = 52$ ppm and *ca.* $\delta = 62$ ppm were observed in the ^{31}P NMR spectrum of dendrimers **TD1–2** for their [$_3$(O)]–P=S and [$_2$(O)N]–P=S bonds, respectively.

A supplementary manifestation of the restricted molecular mobility effect (on the time scale of NMR) due to the increasing molecular weight of members of the series above G_2 was the appearance of a new doublet at *ca.* $\delta = 59$ ppm in the ^{31}P NMR spectra of dendrimers **TD3–5**. Indeed, this new doublet can be interpreted as the NMR signature of two types of non-equivalent [$_2$(O)N]–P=S bonds, resulting from differently crowded and constrained chemical environments to those found in **TD0–2**.

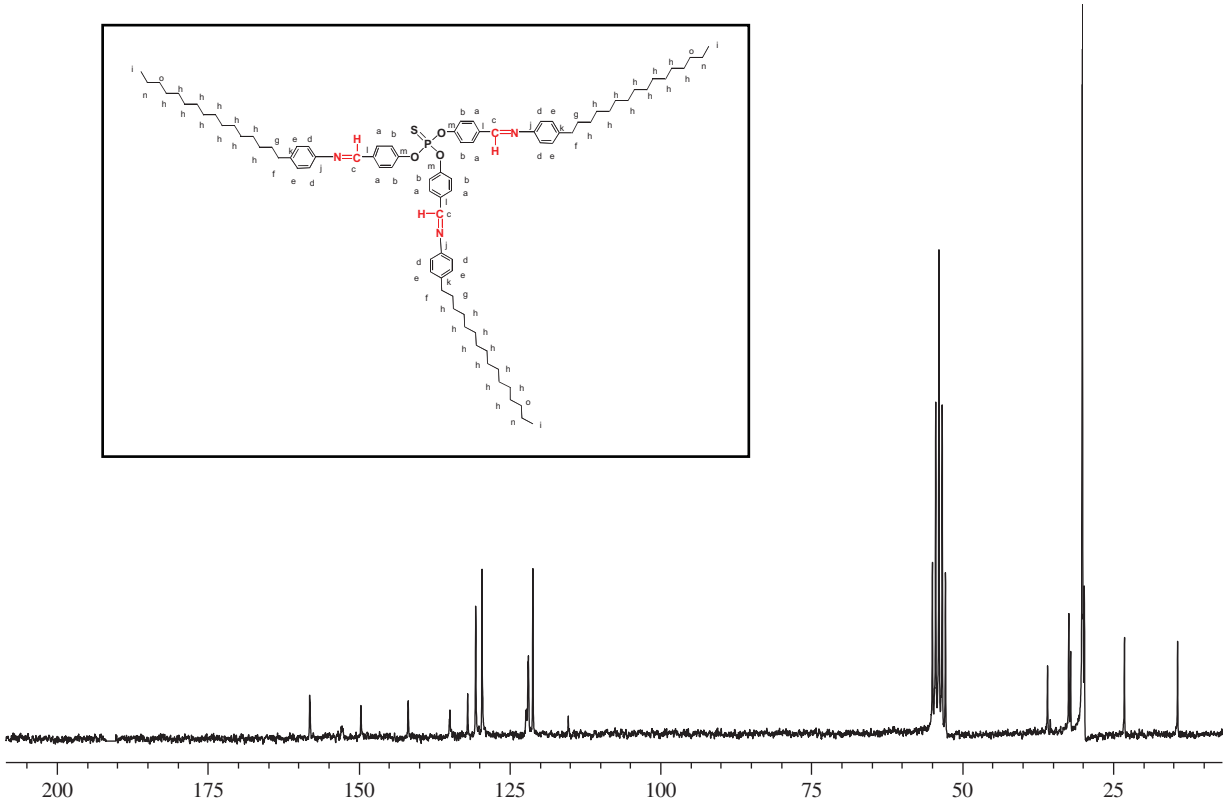

Figure 3. ^{13}C NMR spectrum of thiophosphoryl-PMMH-based LC dendrimer **TD0**. Inset: Chemical structure of **TD0** together with codes related to observed ^{13}C NMR peaks (colour version online).

Final proof of the chemical structures of the series of LC dendrimers **TD0–5** was obtained from their FTIR spectra. Indeed, the disappearance of the typical IR band of CHO surface groups of the dendritic substrates with a maximum at *ca.* 1692 cm^{-1} (for thiophosphoryl-PMMH-6 to thiophosphoryl-PMMH-96 dendrimers of generations $G_{1.5}$–$G_{5.5}$) and at *ca.* 1673 cm^{-1} (for the thiophosphoryl-PMMH-3 dendrimer of generation G_0) at the expense of a new IR band appearing at *ca.* 1624–1628 cm^{-1} confirmed the full conversion of the aldehyde surface reactive functions into azomethine (–CH=N–) bonds [48]. Moreover, the appearance of two typical bands associated with asymmetric and symmetric stretching vibrations of CH_2 groups, located at *ca.* 2919–2916 cm^{-1} and *ca.* 2850–2847 cm^{-1}, of increasing intensity with dendrimers **TD0–5** with increasing generation numbers, provided further evidence of the incorporation of 3–96 *n*-HDA units at the periphery of the LC dendrimers **TD0–5**.

Identification of the mesophases displayed by the LC dendrimers **TD0–5** was performed by POM. The mesophase assignment was based on the observation of fluid and birefingent textures under POM conditions. Phase transitions (and associated enthalpies) shown by the series **TD0–5** were determined by DSC and are summarised in Table 2. The tentative identification of mesophases and the sequence of phase transitions related to dendrimers **TD0–5** has been based on the identification of textures appearing in two reference manuals of liquid crystals [59, 60] and on repeated POM and DSC experiments.

DSC thermograms obtained during the second heating and cooling cycles of each of the LC dendrimers **TD0–5** are shown in Figure 4.

LC dendrimers **TD0** and **TD1** showed similar enantiotropic phase transitions during heating and cooling scans carried out at 0.5 and 0.2°C min^{-1}, respectively. For dendrimers **TD2–5**, disentangling the overlapping Cr→mesophase and mesophase→isotropic transitions required the use of unusually low heating and cooling rates (down to *ca.* 0.01°C min^{-1}) and/or annealing procedures (see Table 2, above).

Using a heating rate of 10°C min^{-1}, melting points of *ca.* 41°C and 50°C were determined for **TD0** and **TD1**, respectively. Melting points of the higher generation dendrimers **TD2–5** were almost constant, all values falling within the range 51–53°C. A similar pattern was observed with the clearing points (i.e. the temperature at which the mesophases formed after the melting disappeared through an isotropisation process) of the LC dendrimers (Table 2). Glass transition temperatures of dendrimers **TD0** and **TD1,** measured

Table 2. Thermal transitions, and corresponding enthalpies, detected by DSC for thiophosphoryl-PMMH- based LC dendrimers up to the fifth generation.

	Temperatures of phase transitions [°C] and corresponding enthalpy changes [J g^{-1}]	
Code	Heating	Cooling
TD0*	35.7 (37.0), 39.7 (28.9), 61.8 (29.5)	31.4 (37.3)
TD1**	42.4 (55.1), 47.9 (16.2), 69.8 (3.5)	31.1, 36.7 (56.7), 53.4 (3.3)
TD2**	38.4 (1.1), 40.4 (1.9), 44.8 (3.8), 50.7 (49.8)	42. 9, 40.7 (123.3)
TD3***	39.1 (0.7), 48.5, 50.6 (106.5)	31.1 (39.4), 46.5 (113.7), 51.4 (25.9)
TD4****	36.8 (4.9), 49.8, 51.0 (121.4)	39.6 (44.7), 45.4 (7.6), 45.7 (76.8),
TD5*****	45.7 (8.0), 51.1, 51.4 (124.2)	47.6, 48.3 (148.4), 49.3 (4.1), 50.49 (1.9)

Notes: *Cooling and heating scans performed at 0.20°C min^{-1}, ** cooling and heating scans performed at 0.25°C min^{-1}, *** heating scan performed at 0.50°C min^{-1}, cooling scan at 0.01°C min^{-1}, **** heating scan at 0.05°C min^{-1} and cooling scan at 0.01°C min^{-1}, ***** cooling and heating scans at 0.01°C min^{-1}.

during the second heating scan (at 20°C min^{-1}) following quenching to −90°C after first heating to 100°C, revealed values of *ca.* −21 +/−10 °C and −34 +/−10 °C, respectively.

All the LC dendrimers **TD0–5** displayed fluid and birefringent textures compatible with smectic mesophases. Even after extensive annealing procedures aimed at better revealing the mesophase, however, the typical smectic-type defects observed during POM observations were unfortunately too small to be unequivocally identified as typical of a smectic mesophase [59–60] of molecular or macromolecular liquid crystals. This reflected a frequently observed situation in the POM imaging of LC dendrimers [30–38], which with increasing generation number (and therefore molecular weight) and despite their intrinsically molecular character by comparison with LC (co)polymers, frequently suffer from small defects. These prevent their attribution to a particular type of mesophase, even after extensive annealing procedures within the mesophase. This is another manifestation (see above) of the inherently restricted molecular mobility which impedes the ease of formation of large-scale supramolecular LC domains in the series **TD0–5**, in which molecular weight increases from 1300 g mol^{-1} to 60 000 g mol^{-1}.

Final attribution to a particular type of smectic mesophase is awaiting detailed temperature-dependent wide-angle X-ray diffraction and small angle X-ray scattering measurements, and this will be the subject of future studies. Meanwhile, the present authors are inclined to attribute the textures observed in this series of LC dendrimers to a disordered smectic mesophase; these have similar features (fluidity and defects) to the classic smectic textures [59–60] of molecular and macromolecular LCs.

Photomicrographs of the birefringent optical textures of the disordered smectic mesophases obtained for LC dendrimers **TD0** and **TD1** are shown in Figure 5.

Based on the published literature related to LC dendrimers with different cores but functionalised at their surface by pro-mesogenic or mesogenic groups [30–38], and the set of DSC and POM data acquired during the present study, it seems that disordered lamellar-type smectic A or C organisations are the most plausible assignments for the mesophases exhibited by the series of LC dendrimers up to the fifth generation.

Based on detailed DSC characterisation and POM observation, one can rationalise the thermal behaviour of the series **TD0–5** as follows. Their clearing temperatures initially increase with generation number, as seen when comparing the clearing temperatures of **TD0** *vs* **TD1** (62°C *vs* 69°C), and subsequently decrease through the second to the fifth generations, all showing clearing temperatures within the range 53–51°C. This leads to a related variation in the temperature range over which this series of LC dendrimers shows a disordered smectic mesophase. In consequence, the temperature extension of the mesophase presented by dendrimers **TD0–5** was seen to be 30.5°C (**TD0**), 35°C (**TD1**), 8.0°C (**TD2** and **3**), and 4.5°C (**TD4** and **5**).

The clearing points of the series of LC dendrimers cannot directly be related to the increase in generation number. This observation is not restricted to thiophosphoryl-PMMH core-based LC dendrimers but is also seen in other LC dendrimer series based on different cores [30–38, 61]. Two mains reasons can be advanced for this unexpected behaviour. Firstly, one must allow for the fact that the chemical structure (and intrinsic rigidity) of the thiophosphoryl-PMMH-core-based LC dendrimers undergoes a dramatic change between **TD0** (with only one S = P–$[O]_3$ focal point and no junctions) and **TD1** (with one S = P–$[O]_3$ focal point and three junctions in the $-\overset{CH_3}{\underset{|}{N}}-\overset{S}{\overset{\|}{P}}-[O]_3$ bond). Although the number of junctions increases significantly (from 3

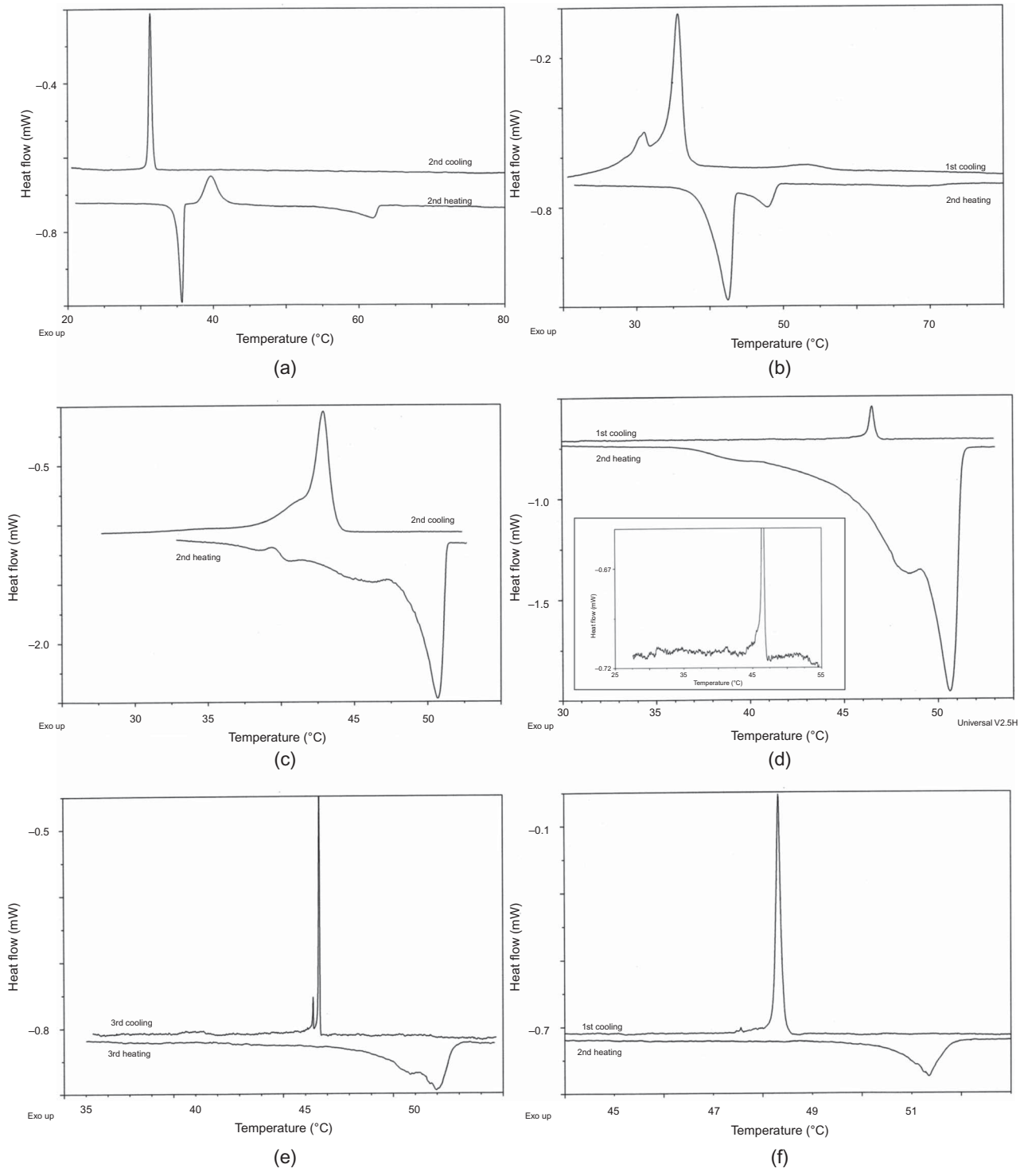

Figure 4. DSC thermograms of the thiophosphoryl-PMMH-core based LC dendrimers of the G_0 – G_5 generations: (a) **TD0** (2nd cooling and heating at 0.2°C min^{-1}), (b) **TD1** (1st cooling and 2nd heating at 0.25°C min^{-1}), (c) **TD2** (2nd cooling at 0.25°C min^{-1} and 2nd heating at 0.25°C min^{-1}), (d) **TD3** (1st cooling at 0.01°C min^{-1} and 2nd heating at 0.5°C min^{-1}), inset (cooling 0.01 deg min^{-1}), (e) **TD4** (3rd cooling at 0.01°C min^{-1} and 3rd heating at 0.05°C min^{-1}), (f) **TD5** (1st cooling at 0.01°C min^{-1} and 2nd heating at 0.01°C min^{-1}).

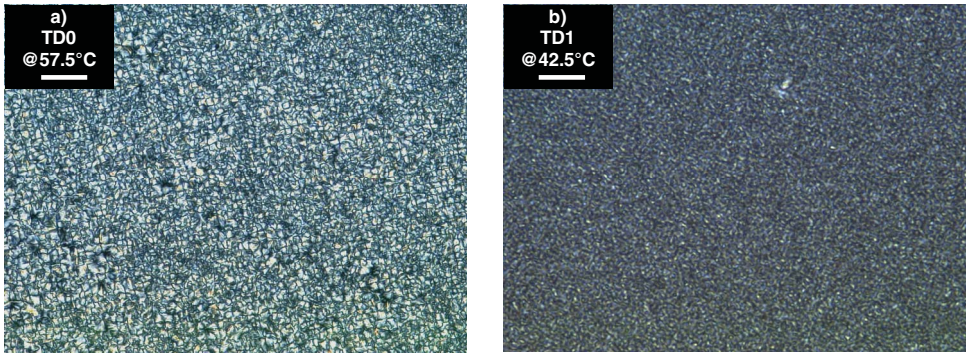

Figure 5. Polarised light optical photomicrographs of the birefringent optical textures of the smectic mesophase displayed by thiophosphoryl-PMMH-based LC dendrimers of the G_0 and G_1 generations: (a) **TD0** (magnification ×20; the scale bar represents 50 μm) and (b) **TD1** (magnification ×20; the scale bar represents 19 μm) (colour version online).

to 93) between **TD2** and **TD5**, no other major chemical changes occur. Secondly, a simple calculation based on the results in Table 1 shows that the azomethine-based pro-mesogenic groups represent 71.3, 58.7, 53.9, 51.8, 50.8 and 50.3 wt% of the total molecular weight of the LC dendrimers **TD0–TD5**, respectively. The thermal behaviour of the thiophosphoryl-PMMH core-based LC dendrimers investigated in this study is thus a complex balance between the effect of their expanding core and those of the pro-mesogenic groups on their surface. **TD2–TD5** have a similar weight content of surface pro-mesogenic groups in relation to molecular weight, typical of oligomer and polymer LCs, increasing from 7012 g mol^{-1} to 60,087 g mol^{-1}. On the other hand, **TD1** and **TD0** have a higher content of surface pro-mesogenic groups in relation to molecular weight (i.e. 3221 g $mol^{-1}$and 1325 g mol^{-1}, typical of molecular LCs). In the present authors' opinion this analysis is supported by the fact that the clearing point of **TD1** is higher than that of **TD0** and that the clearing points of **TD2**–**TD5** all fall within the range 51–53°C.

In support of the tentative scenario regarding the evolution of their clearing points, it has also been observed that an unexpected variation in the enthalpy of isotropisation of LC dendrimers **TD0–5** occurs with increasing generation number when expressed as KJ mol^{-1} per mesogen. Indeed, allowing for a molecular weight of *ca.* 315 g mol^{-1} for the azomethine pro-mesogenic group, calculations lead to 7.420, 0.181, 0.592, 0.304, 0.085 and 0.021 kJ mol^{-1} per mesogen for **TD0–5**, respectively.

The post-functionalisation of commercially available thiophosphoryl-phenoxymethyl(methylhydrazono) dendritic cores containing 3, 6, 12, 24, 48 and 96 aldehyde surface groups, with the reactive pro-mesogenic *n*-hexadecylaniline building block, gives rise to thiophosphoryl-PMMH-based LC dendritic organic semiconductors (OSCs), namely **TD0–5** decorated at their periphery with 3 to 96 Schiff's base chromophores [48]. In solution in THF their UV–Vis spectra display one, two or three more or less well-defined absorption maxima or humps, depending on the generation number of the dendrimer. In particular, in the case of thiophosphoryl-PMMH-based LC dendritic OSC **TD0** it is observed that embedding three azomethine-based chromophores at its periphery gives a well-defined absorption band at 328 nm, typical of azomethine-based OSCs of relatively high band gap (i.e. >3.0 eV).

Despite the increasing number (6 to 96) of optically absorbing azomethine-based chromophores located at the periphery of dendrimers **TD1–5**, Figure 6 shows that their UV–Vis spectra tend to be dominated by a deep UV-absorbing band with maximum at *ca.* 284 nm, converting the clearly resolved band related to the peripheral azomethine-based chromophore [48] seen in the UV–Vis spectrum of **TD0** into humps with maxima at *ca.* 328 nm. These spectroscopic observations illustrate the molecular engineering approach developed in the present study, in which a post-functionalisable phosphorus-based dendritic core has been used as a scaffold for varying numbers (3 to 96) of optically active chromophores within dendritic OSCs up to the fifth generation [56, 57]. Upon excitation at 325 nm, appropriately diluted THF solutions of LC dendritic organic semiconductors **TD0–5** emitted in the UV region of the spectrum (Figure 6), showing a tunable emission band with maxima spanning the 351–369 nm wavelength range [55]. The UV–Vis and PL parameters (absorption maximum (λ_{max}), emission maximum ($\lambda_{em.}$), Stokes shift and optical band gap (E_g^{opt})) from the optical characterisation [55] of the series of thiophosphoryl-PMMH-based LC dendritic organic semiconductors **TD0–5** are summarised in Table 3.

Capitalising on the availability of the high bandgap thiophosphoryl-PMMH-based dendrimers **TD0–5**, a series of OLED devices was fabricated, with an Alq_3

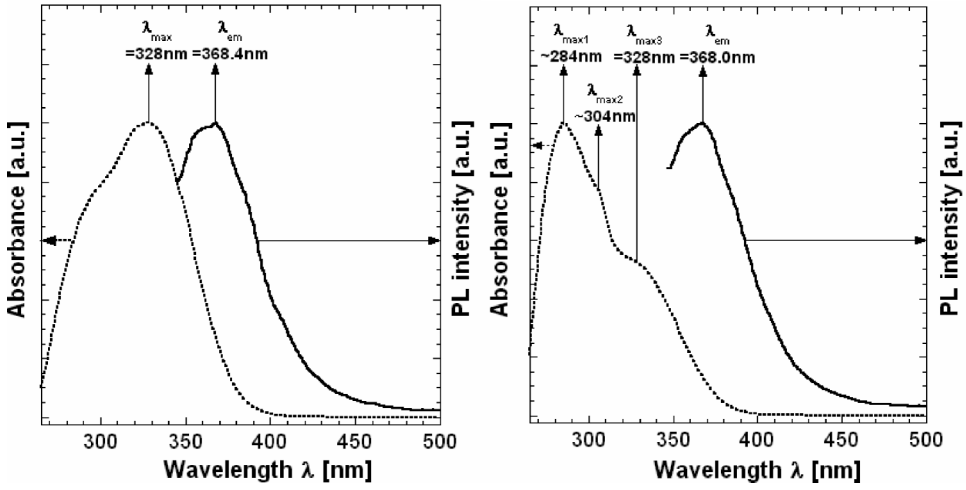

Figure 6. Solution absorption (UV–Vis) and photoluminescence (PL) emission spectra ($\lambda_{exc.} = 325$ nm) of (a) **TD0** and (b) **TD5**. Solvent: THF.

Table 3. Optoelectronic features (absorption maximum (λ_{max}), maximum of emission ($\lambda_{em.}$), Stokes shift, optical band gap (E_g^{opt})) of the series of thiophosphoryl-PMMH-based LC dendrimers up to the fifth generation.

Code	λ_{max} [nm]/[eV]	$\lambda_{em.}$ [nm]/[eV]	Stokes shift [nm]/[cm^{-1}]*	E_g^{opt} [eV]
TD0	284h,328/4.37, 3.78	368/3.37	40/3314	3.26
TD1	284, 328/4.37, 3.78	368/3.37	40/3314	3.26
TD2	284, 328/4.37, 3.78	368/3.37	40/3314	3.26
TD3	284, 328/4.37, 3.78	369/3.36	41/3387	3.26
TD4	284, 328/4.37, 3.78	351/3.53	23/1997	3.26
TD5	284, 328/4.37, 3.78	358/3.46	30/2555	3.26

Notes: *$\nu_{abs.} - \nu_{emis.} = (1/\lambda_{max.} - 1/\lambda_{em.}) \times 10^7$ [cm^{-1}]

green-emitting layer serving as reference OLED, and OLEDs with an additional HTL consisting of a thin film of a dendrimer **TD0–5** [56, 57] inserted between the ITO anode and the Alq_3 green-emitting layer. Selected IV characteristics of two OLEDs having multi-layered ITO/dendrimer **TD0** or dendrimer **TD5**/Alq_3/Al architecture are shown in Figure 7.

The turn-on voltage values obtained for the two OLEDs using HTL layers consisting of thiophosphoryl-PMMH-based dendrimers **TD0** and **TD5** were *ca.* 5.0 V, and consequently lower by 1.0–2.0 V than the turn-on voltage value determined for the reference OLED (not shown here). These preliminary results indicate that, irrespective of their generation numbers, high band-gap and thermostable [17] thiophosphoryl-PMMH-based dendrimers hold potential for providing a new generation of efficient dendritic hole transporting materials for OLEDs. Additionally, it is anticipated that they could play a similarly useful role as the polystyrene-doped poly(3,4-ethylenedioxythiophene) thin layer often used in high performance OLEDs as a buffer layer against the deleterious diffusion of indium, and/or tin, and/or oxygen from the

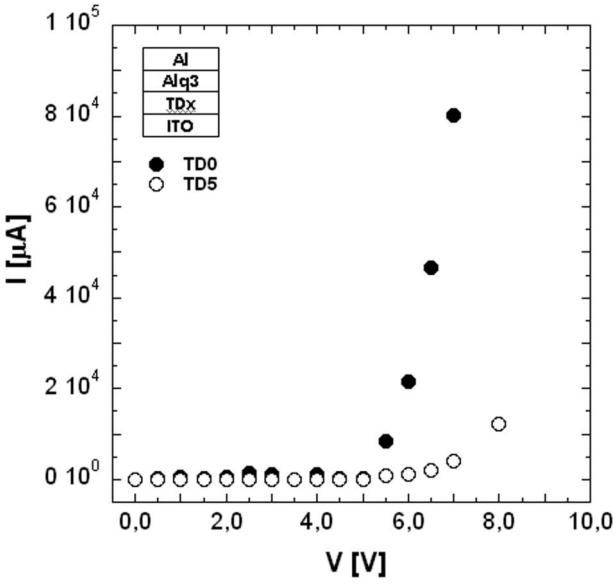

Figure 7. Current–voltage (*IV*) characteristics of OLED devices using Alq_3 and generation G_0 (filed black circle) *vs* generation G_5 (open black circle) thiophosphoryl-PMMH-based LC dendrimers as emitting and hole transporting layer, respectively. Inset: Schematic sketch of the multilayer architecture of the OLEDs studied.

ITO anode, into the emissive layer of this type of optoelectronic device [62]. The present study therefore suggests a potential new application for phosphorus-based dendrimers by exploiting their hole (or electron) transporting properties which supplement the already reported use of appropriately core/shell/periphery-functionalised dendrimers [56, 57] as emissive materials for OLEDs [23, 63, 64], paving the way towards stable organic optoelectronic devices (e.g. solar cells) using dendrimer based-HTLs, emissive layers, and electron transporting layers.

4. Conclusions

A series of thermotropic LC dendrimers up to the fifth generation, based on a thiophosphoryl-phenoxymethyl(-methylhydrazono) dendritic core and decorated at their periphery with 3 to 96 azomethine-based chromophoric units, have been synthesised and characterised. These LC dendritic organic semiconductors all exhibit a disordered smectic mesophase, with tunable temperature extension of the mesomorphic state, as a function of generation number. By virtue of the tunable surface content of optically active azomethine-based chromophore units, the phosphorus-based dendrimers **TD0–5** are high band-gap optoelectronically active organic semi-conductors emitting in the UV region of the spectrum. They can also be used as hole transporting materials in multilayered organic LEDs. The successful molecular engineering approach developed for the generation of this series of dendritic organic semiconductors, showing tunable mesomorphic behaviour and (opto)electronic properties, allows a range of valuable organic semiconductors to be produced for use in optically and/or electronically active layers in other (opto)electronic devices. These include field-effect transistors, solar cells and lasers.

Acknowledgements

One of the authors (AI) is grateful to the Chemistry Department of CNRS for the funding of her one-year post-doctoral fellowship within the UMR5819–SPrAM (CEA/CNRS/Univ. J. FOURIER-Grenoble I) laboratory. The authors also wish to thank P.-A. Bayle and M. Bardet of the Laboratoire de Résonance Magnétique of INAC/CEA-Grenoble for their assistance with the ^{31}P NMR spectroscopic characterisation of the thiophosphoryl-PMMH-based LC dendritic organic semiconductors.

References

[1] Buhleier, E.W.; Wehner, W.; Vögtle, F. *Synthesis* **1978**, *2*, 155–158.
[2] Tomalia, D.A.; Baker, H.; Dewald, J.; Hall, M.; Kallos, G.; Martin, S.; Roeck, J.; Ryder, J.; Smith, P. *Polym. J.* **1985**, *17*, 117–132.
[3] Newkome, G.R.; Yao, Z.; Baker, G.R.; Gupta, V.K. *J. Org. Chem.* **1985**, *50*, 2003–2004.
[4] Hawker, C.J.; Fréchet, J.M.J. *J. Am. Chem. Soc.* **1990**, *112*, 7638–7647.
[5] Miller, T.M.; Neenan, T.X. *Chem. Mater.* **1990**, *2*, 346–349.
[6] Graysson, S.M.; Fréchet, J.M.J. *Chem. Rev.* **2001**, *101*, 3819–3868.
[7] Tomalia, D.A.; Fréchet, J.M.J. *J. Polym. Sci., Part A: Polym. Chem.* **2002**, *40*, 2719–2728.
[8] Tomalia, D.A. *Prog. Polym. Sci.* **2005**, *30*, 293–324.
[9] Tomalia, D.A. *Mater. Today* **2005**, *8*, 34–46.
[10] Launay, N.; Caminade, A.-M.; Majoral, J.-P. *J. Organomet. Chem.* **1997**, *529*, 51–58.
[11] Lartigue, M.L.; Donnadieu, B.; Galliot, C.; Caminade, A.-M.; Majoral, J.-P. *Macromolecules* **1997**, *30*, 7335–7337.
[12] Majoral, J.-P.; Caminade, A.-M. *Chem. Rev.* **1999**, *99*, 845–880.
[13] Turrin, C.-O.; Maraval, V.; Caminade, A.-M.; Majoral, J.-P.; Mehdi, A.; Reyé, C. *Chem. Mater.* **2000**, *12*, 3848–3856.
[14] Majoral, J.-P.; Caminade, A.-M.; Maraval, V. *Chem. Commun.* **2002**, 2929–2942.
[15] Caminade, A.-M.; Maraval, V.; Laurent, R.; Turrin, C.-O.; Sutra, P.; Leclaire, J.; Griffe, L.; Marchand, P.; Baudoin-Dehoux, C.; Rebout, C.; Majoral, J.-P. *C. R. Chim.* **2003**, *6*, 791–801.
[16] Trevisiol, E.; Le Berre-Anton, V.; Leclaire, J.; Pratviel, G.; Caminade, A.-M.; Majoral, J.-P.; Francois, J.M.; Meunier, B. *New J. Chem.* **2003**, *27*, 1713–1719.
[17] Turrin, C.-O.; Maraval, V.; Leclaire, J.; Dantras, E.; Lacabanne, C.; Caminade, A.-M.; Majoral, J.-P. *Tetrahedron* **2003**, *59*, 3965–3973.
[18] Leclaire, J.; Coppel, Y.; Caminade, A.-M.; Majoral, J.-P. *J. Am. Chem. Soc.* **2004**, *126*, 2304–2305.
[19] Caminade, A.-M.; Majoral, J.-P. *Acc. Chem. Res.* **2004**, *37*, 341–348.
[20] Marchand, P.; Griffe, L.; Caminade, A.-M.; Majoral, J.-P.; Destarac, M.; Leising, F. *Org. Lett.* **2004**, *6*, 1309–1312.
[21] Kanibolotsky, A.; Roquet, S.; Cariou, M.; Leriche, P.; Turrin, C.-O.; de Bettignies, R.; Caminade, A.-M.; Majoral, J.-P.; Khodorkovsky, V.; Gorgues, A. *Org. Lett.* **2004**, *6*, 2109–2112.
[22] Caminade, A.-M.; Maraval, A.; Majoral, J.-P. *Eur. J. Inorg. Chem.* **2006**, *5*, 887–901.
[23] Brauge, L.; Vériot, G.; Franc, G.; Deloncle, R.; Caminade, A.-M.; Majoral, J.-P. *Tetrahedron* **2006**, *62*, 11891–11899.
[24] Servin, P.; Rebout, C.; Laurent, R.; Peruzzini, M.; Caminade, A.-M.; Majoral, J.-P. *Tetrahedron Lett.* **2007**, *48*, 579–583.
[25] Caminade, A.-M.; Servin, P.; Laurent, R.; Majoral, J.-P. *Chem. Soc. Rev.* **2008**, *37*, 56–67.
[26] Caminade, A.-M.; Turrin, C.-O.; Majoral, J.-P. *Chem. Eur. J.* **2008**, *14*, 7422–7432.
[27] Caminade, A.-M.; Wei, Y.Q.; Majoral, J.-P. *C. R. Chim.* **2009**, *12*, 105–120.
[28] Rolland, O.; Turrin, C.-O.; Caminade, A.-M.; Majoral, J.-P. *New J. Chem.* **2009**, *33*, 1809–1824.

[29] Caminade, A.-M.; Hameau, A.; Majoral, J.-P. *Chem. Eur. J.* **2009**, *15*, 9270–9285.
[30] Marcos, M.; Omenat, A.; Serrano, J.L. *C. R. Chim.* **2003**, *6*, 947–957.
[31] Kumar, S. *Liq. Cryst*. **2004**, *31*, 1037–1059.
[32] Barberá, J.; Donnio, B.; Gehringer, L.; Guillon, D.; Marcos, M.; Omenat, A.; Serrano, J.L. *J. Mater. Chem.* **2005**, *15*, 4093–4015.
[33] Donnio, B.; Guillon, D. *Adv. Polym. Sci.* **2006**, *201*, 45–155.
[34] Donnio, B.; Buathong, S.; Bury, I.; Guillon, D. *Chem. Soc. Rev.* **2007**, *36*, 1495–1513.
[35] Marcos, M.; Martin-Rapun, R.; Omenat, A.; Serrano, J.L. *Chem. Soc. Rev.* **2007**, *36*, 1889–1901.
[36] Goodby, J.W.; Saez, I.M.; Cowling, S.J.; Gasowska, J.S.; MacDonald, R.A.; Sia, S.; Watson, P.; Toyne, K.J.; Hird, M.; Lewis, R.A.; Lee, S.-E.; Vaschenko, V. *Liq. Cryst.* **2009**, *36*, 567–605.
[37] Imrie, C.T.; Henderson, P.A.; Yeap, G.-Y. *Liq. Cryst.* **2009**, *36*, 755–777.
[38] Moriya, K.; Suzuki, T.; Yano, S.; Kajiwara, M. *Liq. Cryst.* **1995**, *18*, 795–800.
[39] Moriya, K.; Nakagawa, S.; Yano, S.; Kajiwara, M. *Liq. Cryst.* **1995**, *18*, 919.
[40] Moriya, K.; Mizusaki, H.; Kato, M.; Suzuki, T.; Yano, S.; Kajiwara, M.; Tashiro, K. *Chem. Mater.* **1997**, *9*, 255–263.
[41] Moriya, K.; Suzuki, T.; Kawanishi, Y.; Masuda, T.; Mizusaki, H.; Nakagawa, S.; Ikematsu, H.; Mizuno, K.; Yano, S.; Kajiwara, M. *Appl. Organomet. Chem*. **1998**, *12*, 771–779.
[42] Moriya, K.; Kawanishi, Y.; Yano, S.; Kajiwara, M. *Chem. Commun.* **2000**, 1111–1112.
[43] Moriya, K.; Suzuki, T.; Yano, S.; Miyajima, S. *J. Phys. Chem. B* **2001**, *105*, 7920–7927.
[44] Moriya, K.; Ikematsu, H.; Nakagawa, S.; Yano, S.; Negita, K. *Jpn. J. Appl. Phys.* **2001**, *40*, L340–L342.
[45] Barbera, J.; Bardaji, M.; Jimenez, J.; Laguna, A.; Pilar Martinez, M.; Oriol, L.; Serrano, J.L.; Zaragozano, I. *J. Am. Chem. Soc.* **2005**, *127*, 8994–9002.
[46] Barbera, J.; Jimenez, J.; Laguna, A.; Oriol, L.; Perez, S.; Serrano, J.L. *Chem. Mater.* **2006**, *18*, 5437–5445.
[47] Xu, J.; Ling, T.C.; He, C. *J. Polym. Sci. Part A: Polym. Chem.* **2008**, *46*, 4691–4703.
[48] Tidwell, T.T. *Angew. Chem., Int. Ed.* **2008**, *47*, 1016–1020.
[49] Singler, R.E.; Willingham, R.A.; Lenz, R.W.; Furukawa, A.; Finkelmann, H. *Macromolecules* **1987**, *20*, 1727–1728.
[50] Kim, C.; Allcock, H.R. *Macromolecules* **1987**, *20*, 1726–1727.
[51] Kumaresan, S.; Kannan, P. *J. Polym. Sci.: Part A: Polym. Chem.* **1988**, *41*, 3188–3196.
[52] Allcock, H.R.; Kim, C. *Macromolecules* **1989**, *22*, 2596–2602.
[53] Allcock, H.R.; Kim, C. *Macromolecules* **1990**, *23*, 3881–3887.
[54] Allcock, H.R.; Klingenberg, E.H. *Macromolecules* **1995**, *28*, 4351–4360.
[55] Ceroni, P.; Bergamini, G.; Marchioni, F.; Balzani, V. *Prog. Polym. Sci.* **2005**, *30*, 453–473.
[56] Lo, S.-C.; Burn, P.L. *Chem. Rev.* **2007**, *107*, 1097–1116.
[57] Hwang, S.-H.; Moorefield, C.N.; Newkome, G.R. *Chem. Soc. Rev.* **2008**, *37*, 2543–2557.
[58] Forrest, S.R. *Nature* **2004**, *428*, 911–918.
[59] Demus, D.; Richter, L. *Textures of Liquid Crystals*, 1st ed; Leipzig: Verlag Chemie, 1978.
[60] Gray, G.W.; Goodby, J.W. *Smectic Liquid Crystals: Textures and Structures*; Glasgow & London: Leonard Hill, 1984.
[61] Barberá, J.; Marcos, M.; Serano, J.L. *Chem. Eur. J.* **1999**, *5*, 1834–1840.
[62] de Jong; M.P.; van Jzendoorn, L.J.; de Voigt, M.J.A. *Appl. Phys. Lett.* **2000**, *77*, 2255–2257.
[63] Bolink, H.J.; Santamaria, S.G.; Sudhakar, S.; Zhen, C.; Sellinger, A. *Chem. Commun.* **2008**, 618–620.
[64] Bolink, H.J.; Barea, E.; Costa, R.D.; Coronado, E.; Sudhakar, S.; Zhen, C.; Sellinger, A. *Org. Electron.* **2008**, *9*, 155–163.